Research Article

Optimization of Friction Stir Welding Parameters for Dissimilar Joining of Aluminum Alloy 2024 and Magnesium Alloy AZ91C Using Taguchi Method

S. Rouhi[1], A. Doniavi[1*] and M. Shahbaz[2*]

[1] Department of Mechanical Engineering, Faculty of Engineering, Urmia University, Urmia, Iran
[2] Department of Materials Science and Engineering, Faculty of Engineering, Urmia University, Urmia, Iran

ARTICLE INFO

ABSTRACT

In this research, friction stir welding (FSW), a solid-state joining process, was employed to weld 5 mm thick sheets of aluminum alloy Al2024 and magnesium alloy AZ91C. The Taguchi design of experiments method was utilized to optimize the FSW process parameters including tool rotational speed (800-1600 rpm), welding speed (8-20 mm/min), and plunge depth (0.2-0.4 mm) to achieve maximum hardness in the weld zone. Microstructural characterization was studied using optical and scanning electron microscopes. The optimum parameters were found to have a 1600 rpm rotational speed, 8 mm/min welding speed, and 0.4 mm plunge depth, resulting in a maximum hardness of 148 HV in the stir zone (SZ). The layered or onion ring structure observed in the SZ was attributed to insufficient mixing and elemental diffusion between the dissimilar alloys due to the short interaction time during welding. Scanning electron microscopy revealed the formation of a continuous intermetallic layer at the aluminum-magnesium interface and the dispersion of magnesium particles in the aluminum matrix, contributing to the composite-like structure in certain regions. The hardness variation perpendicular to the weld line was correlated with the microstructural evolution, with the highest hardness observed in the fine-grained SZ due to grain refinement and precipitation hardening. The thermomechanically affected zone (TMAZ) exhibited lower hardness due to the presence of coarser precipitates and partially recrystallized grains. This research demonstrates the feasibility of joining Al2024 and AZ91C alloys using FSW and highlights the importance of optimizing process parameters to achieve desirable mechanical properties and microstructural characteristics in the dissimilar weld joint.

© Shiraz University, Shiraz, Iran, 2024

1. Introduction

The welding of dissimilar alloys and metals poses significant challenges within the welding domain, due to their disparate physical and chemical properties. Conventional welding methods often struggle to effectively join metals with distinct characteristics such as steel, aluminum, copper, and titanium, leading to issues like crack susceptibility and weak mechanical properties in the weld. Friction stir welding (FSW), introduced in 1991 at The Welding Institute of England,

---

emerged as a promising solution within the realm of solid-state welding processes [1]. In FSW, a non-consumable tool with specialized design and rotational movement enters the welding area under defined conditions, generating friction and heat at the contact point with the workpiece [2, 3]. Fig. 1 shows the schematics of the FSW process. This, coupled with a compressive force, facilitates controlled plastic deformation of the material, enabling the mixing and joining of paste-like materials along the weld seam [4].

Various parameters govern the FSW process including tool design, workpiece fixture method, rotational and advancing speeds, tool position, applied pressure, and pin shape, all of which influence material flow patterns and temperature distribution. Material mixing and microstructure distribution play pivotal roles in determining the mechanical behavior of the final joint, with the formation of onion ring-shaped areas being particularly noteworthy [5]. Extensive research has been conducted on FSW technology, exploring the formability of welded dissimilar alloy sheets and examining the mechanical and metallurgical properties of friction stir welded aluminum and magnesium alloy sheets [6].

Aluminum alloy Al2024 and magnesium alloy AZ91C find widespread applications across aerospace, automotive, marine, and aviation industries owing to their favorable mechanical and physical properties [7]. However, welding these dissimilar alloys presents inherent challenges due to their divergent physical, chemical, and metallurgical properties. Previous studies have highlighted the limitations and challenges associated with conventional welding methods, such as gas metal arc welding, when welding Al2024 to AZ91C alloys [1-3].

The literature review presents several notable studies focusing on the optimization of friction stir welding parameters and the examination of dissimilar welds between various alloy combinations. These studies have investigated the effects of tool geometry, process parameters, and alloy compositions on the mechanical and metallurgical properties of friction stir welded joints [8].
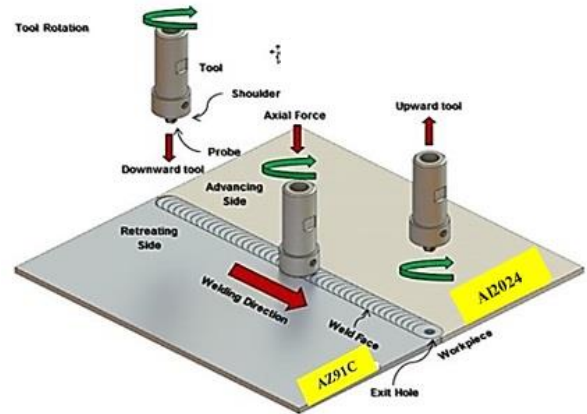

Fig. 1. The schematics of FSW process.

Notably, studies have been conducted on dissimilar welds between Al2024 and Al5052 aluminum alloys, AZ91C magnesium alloy and Al6063 aluminum alloy, as well as A383 aluminum alloy and AZ91 magnesium alloy [9-11].

Despite the increasing demand for welding dissimilar aluminum and magnesium alloys in industrial applications, limited research has been conducted on the weldability of alloys such as Al2024 and AZ91C. Given the potential of FSW to mitigate welding defects, minimize distortion and residual stresses, and induce minimal structural changes, the utilization of this process for welding dissimilar alloys holds promise. Hence, investigating the impact of process parameters and optimizing these conditions to enhance joint quality is of paramount interest to both academic and industrial researchers. This study fills a gap in the existing literature by examining the effect of parameters on the microstructure and mechanical behavior of dissimilar friction stir welded joints between the Al2024 and AZ91C alloys, underscoring the importance of precise parameter optimization to achieve defect-free welds with acceptable mechanical properties. Consequently, this research focuses on optimizing friction stir welding parameters using the Taguchi method to address this critical need.

2. Materials and Methods

Given the importance and existing limitations in welding dissimilar alloys, the need to conduct research in this area using two dissimilar materials was observed. The

Al2024 aluminum alloy and AZ91C magnesium alloy in 5 mm sheets were selected for friction stir welding. These materials are among the most globally used materials in industry [14, 15]. The chemical composition and tensile test data are presented in Table 1 and Table 2, respectively.

Table 1. Chemical composition of base materials

Chemical composition AZ91C (wt. %)							
Mg	**Al**	**Zn**	**Ni**	**Cu**	**Si**	**Fe**	**Mn**
88.97	8.9	0.84	0.87	0.004	0.07	0.01	0.336
Chemical composition Al2024 (wt. %)							
Al	**Cr**	**Cu**	**Fe**	**Mg**	**Mn**	**Si**	**Zn**
92.08	0.01	4.94	0.46	1.76	0.51	0.23	0.01

Table 2. Mechanical properties of base metals

Sample	Yield stress (N/mm^2)	UTS (N/mm^2)	Strain at fracture (%)	Hardness (VHN)
AZ91C	97	131	8.45	49.63
Al2024	349	414	13.65	138.16

The sheets were first machined with a milling machine to dimensions of 150×25×5 mm³ with 0.1 mm precision. By placing two samples next to each other, a welding specimen was prepared so that before welding, the edges were placed completely next to each other without any gap. Fig. 2 shows the dimensions of the workpieces used.

The microstructures of the Al2024 and AZ91C alloys are shown in Fig. 3(a) and 3(b), respectively. As can be observed, the microstructure of Al2024 consists of elongated grains in the aluminum rolling direction with a random distribution of black-colored particles, which can be distinguished as precipitates [12]. The grains in the AZ91C magnesium alloy are slightly coarser and contain more particles compared to the 2024 aluminum alloy [13].
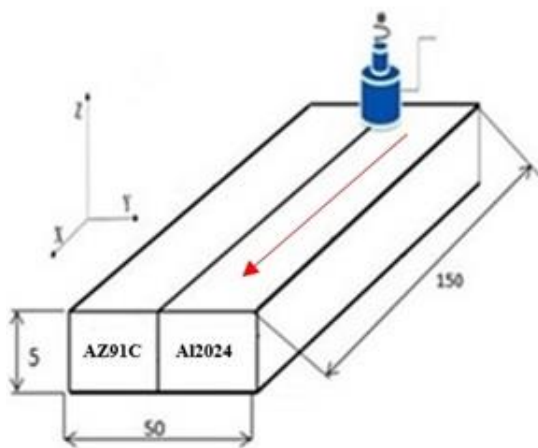
For welding, H13 steel tools were used. Different tool geometries can be employed depending on the type of sheet connection and their thickness. To achieve better material flow during friction and stir welding, the tool pin had a square shape and the tool rotated in a clockwise direction [16, 17].
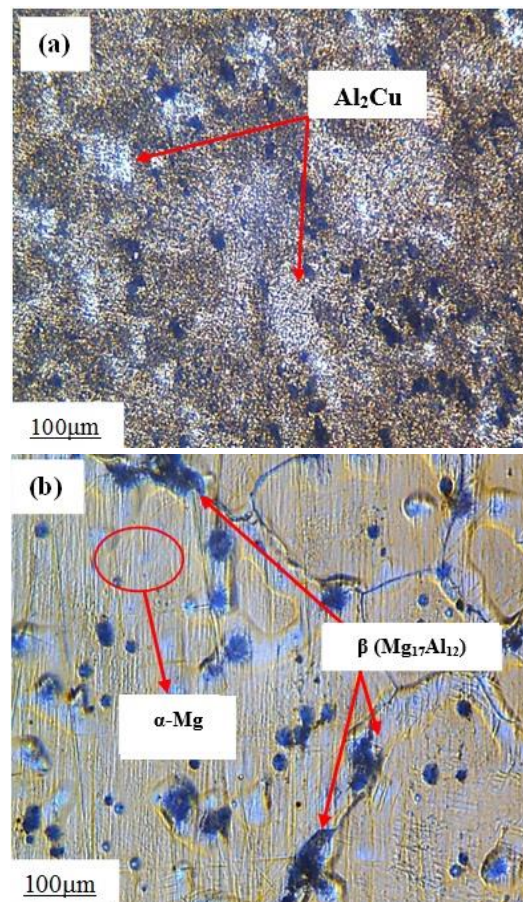

Fig. 2. Dimensions of the used workpieces. (Dimensions are in mm.)

Fig. 3. Base metal microstructures; (a) Al2024 aluminum alloy and (b) AZ91C magnesium alloy.

The forging direction was selected appropriately for material flow behind the tool during welding to achieve a defect-free joint. The tool angle relative to the perpendicular axis was three degrees [18, 19]. A suitable fixture was designed and built to rigidly hold the pieces (Fig. 4(a)). The shoulder diameter of the tool, pin diameter, and pin length are 18 mm, 6 mm (4.25×4.25 mm²), and 4 mm, respectively. To save on tool material, the design is double-sided, as shown in Fig. 4(b), and the pieces are held rigidly. Before welding, the surface was cleaned with an acid solution followed by mechanical abrasion to remove any surface

oxides and impurities [20].

In this study, to conduct experiments and achieve the desired result, the Taguchi design of experiments approach was followed step-by-step. First, process parameters were studied then the response variable, which is hardness of the produced sheet, was determined. The studied parameters are presented in Table 3. The selection of parameters is based on their significance and ranges based on previous research and laboratory facilities, with 9 experiments chosen according to the L9 array shown in Table 4 [21].

Table 3. Process parameters and their levels

Parameter	Range	Level 1	Level 2	Level 3
Tool rotation speed (rpm)	800-1600	800	1250	1600
Velocity (mm/min)	8-20	8	16	20
Plunge depth (mm)	0.2-0.4	0.2	0.3	0.4

Table 4. L9 orthogonal array or input variables

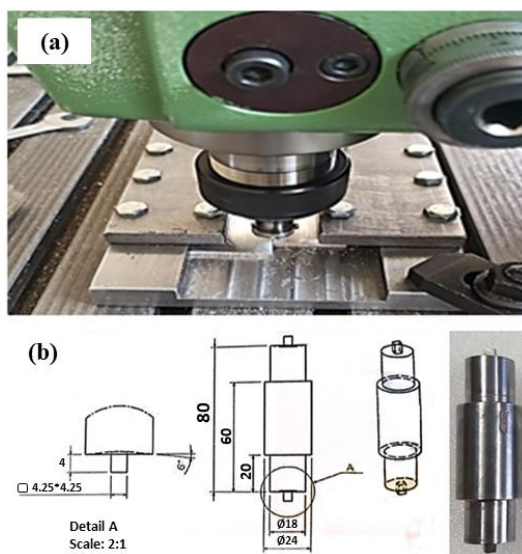| Experiment No.	Tool rotation speed (rpm)	Velocity (mm/min)	Plunge depth (mm)
1	800	8	0.2
2	800	16	0.3
3	800	20	0.4
4	1250	8	0.3
5	1250	16	0.4
6	1250	20	0.2
7	1600	8	0.4
8	1600	16	0.2
9	1600	20	0.3

Fig. 4. (a) Designed fixture for FSW process and (b) dimensions and shape of used tool and method of rigidly holding pieces in FSW process. (Dimensions are in mm.)

After the process, to remove surface effects and irregularities, all pieces were milled to one millimeter. To study the hardness of cross section samples after mechanical polishing, the Vickers microhardness tester was used. Hardness measurement points were chosen at 1 mm distance from the FSWed surface. The hardness of the sample was measured by applying a 100 gf load for 10 seconds [18]. The hardness measurement location is shown in Fig. 5. Metallurgical images from the weld cross section after surface preparation including cutting, mounting, sanding (from #120 to #3000 grit) and polishing, were first etched in a solution containing HF, HNO_3, HCl and H_2O and then in a solution containing acetic acid, ethanol, picric acid and H_2O before imaging [19].
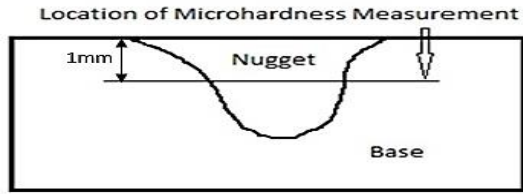
Fig. 5. Microhardness measurement location.

3. Results and Discussion

3.1. Signal to noise ratio

The specimen hardness stands out as the paramount characteristic under scrutiny in this study, serving to delineate the quality of friction stir welded joints through microstructural attributes. To assess the impact of various factors on the response, we computed the signal-to-noise (S/N) ratios and means for each control factor. Signals denote the influence on mean responses, while noises gauge deviations from the experimental run's sensitivity to noise factors. The selection of an appropriate S/N ratio necessitates prior knowledge, expertise, and an understanding of the process. In cases where the objective remains fixed and signal factors are negligible or absent (static design), the choice of signal-to-noise (S/N) ratio can be selected depending on the design goal [21, 22]. In the present study, S/N ratio was selected with respect to the larger-the-better criterion in order to maximize the response.

The experimental results pertaining to microhardness were transformed into means and signal-to-noise ratios (S/N). Specifically, we computed 9 means and 9 S/N ratios, and the resultant hardness estimates, means, and signal-to-noise ratios are presented in Table 5.

Table 5. Orthogonal array for L9 with response (raw data and S/N ratio)

Signal (Input)			Noise (Output)	Ratio	
Tool rotation speed (rpm)	Velocity (mm/min)	Plunge depth (mm)	Hardness (HV)	S/N Ratio	Mean value
800	8	0.2	101	36.1618	75.95
800	16	0.3	105	37.0646	81.25
800	20	0.4	110	37.6918	86.15
1250	8	0.3	131	38.9546	101.20
1250	16	0.4	133	38.8697	101.60
1250	20	0.2	110	38.3733	89.65
1600	8	0.4	148	41.0728	121.55
1600	16	0.2	137	39.3642	105.95
1600	20	0.3	142	39.4610	108.6

Table 6. Main effects of Vickers hardness (means and S/N ratio)

	For S/N ratios			For means		
Level	Tool rotation speed (rpm)	Velocity (mm/min)	Plunge depth (mm)	Tool rotation speed (rpm)	Velocity (mm/min)	Plunge depth (mm)
1	36.76	38.52	37.85	76.28	94.07	87.68
2	38.32	38.16	38.22	87.32	89.27	89.68
3	39.85	38.25	38.86	108.37	88.63	94.60
Delta	3.09	0.35	1.01	32.08	5.43	6.92
Rank	1	3	2	1	3	2

Each experimental analysis furnishes the mean for the optimal combination of parameter levels ensuring a high weld zone hardness based on the experimental dataset. The mean response delineates the average performance characteristic value for each parameter across different levels. Computation of the mean for a given level involves deriving the overall average of all responses at that level. The raw data for mean response and S/N ratio of weld zone hardness for each parameter at levels 1, 2, and 3 were calculated and are summarized in Table 6. Furthermore, Table 6 provides insights into the means and S/N ratios for different process parameters as they transition from lower to higher levels, with higher S/N ratios indicating superior quality characteristics. Consequently, the optimal level of a welding parameter corresponds to the level with the highest S/N ratio. A visual representation comparing mean effect and S/N ratio is depicted in Fig. 6. Utilizing statistical software, we computed the mean effect and S/N ratio for weld zone hardness, revealing that the weld
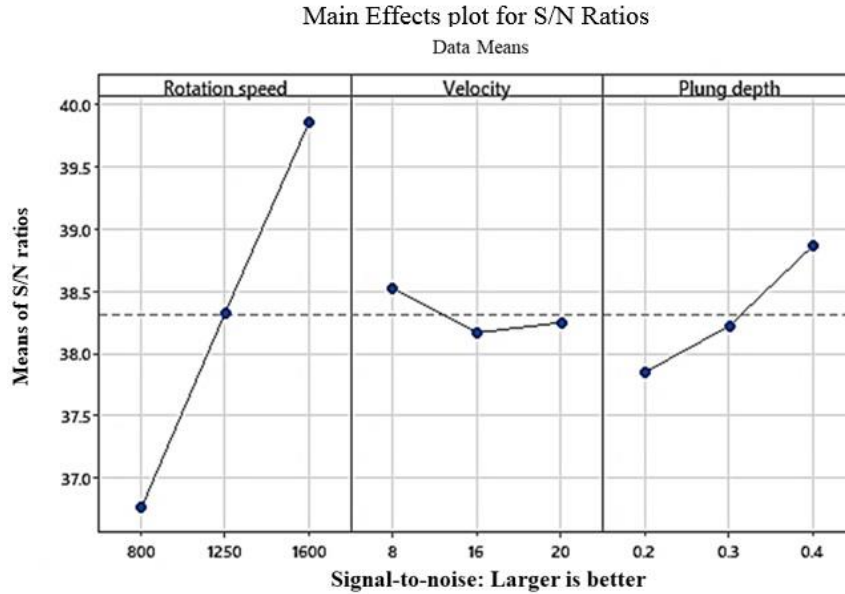
Fig. 6. Comparison of mean effect and S/N ratio.

zone hardness is maximized at rotational speeds of 1600 rpm, Velocity of 8 mm/min, and a depth of penetration of 0.4 mm.

An analysis of variance (ANOVA) was conducted to identify welding parameters that bear statistical significance. The ANOVA test aimed to scrutinize the significance of process parameters impacting friction stir weld hardness [21]. The results of variance analysis for hardness means and S/N ratios are summarized in Table 7.

Table 7. Analysis of variance for Vickers hardness (S/N ratio)

Source	DF	Seq SS	Adj SS	Adj MS	F	P
Tool rotation speed	2	14.3546	14.3546	7.1773	16.85	0.056
Velocity	2	0.2072	0.2072	0.1036	0.24	0.804
Plunge depth	2	1.5804	1.5804	0.7902	1.86	0.350
Residual error	2	0.8519	0.8519	0.4259		
Total	8	16.9941				

Where DF is degree of freedom, Adj SS is adjusted sum of square, Adj MS is adjusted mean square, F is Fisher ratio and P is Probability that exceeds the 95% confidence level.

Additionally, an F-test, named after Fisher, was employed to discern which processes exert a significant effect on weld zone hardness. Generally, a high F-value indicates that changes in the process parameter significantly influence quality characteristics. The ANOVA outcomes underscore the pivotal role played by the welding parameters considered, in order of significance: rotational speed, depth, and welding speed. Consequently, the optimal values for these parameters are provided in Table 8.

Table 8. Optimum welding conditions

Optimum parameter		
Tool rotational speed (rpm)	Velocity (mm/min)	Plunge depth (mm)
1600	8	0.4

3.2. Macrostructure analysis

First, macroscopic images were taken from the cross-section of all samples, which can be observed in Table 9. As seen in Table 9, samples at high traverse speeds have defects that are eliminated with decreasing traverse speed. On the other hand, with increasing heat input, at high rotational and traverse speeds, defects are observed in the magnesium metal matrix. It can be said that among these samples, the highest visual quality belongs to sample 7

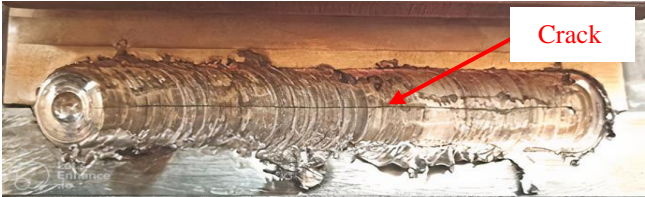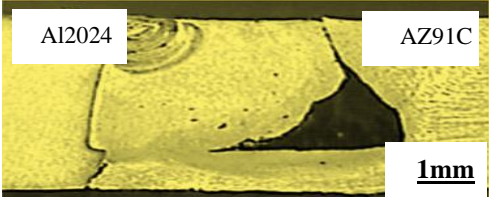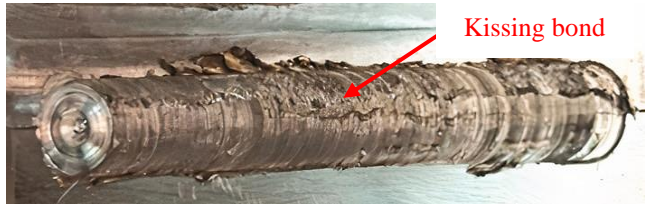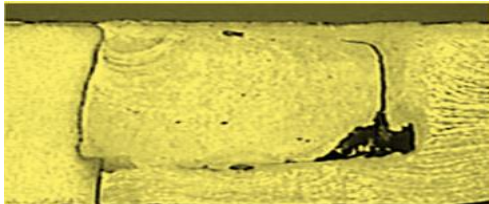**Table 9.** Final dissimilar FSW profile and macrostructure of Al2024 and AZ91C alloys
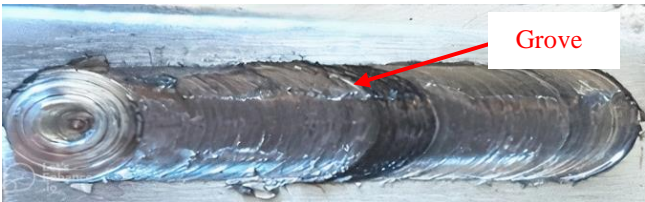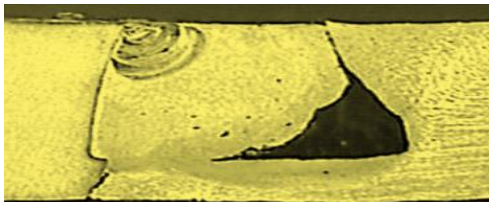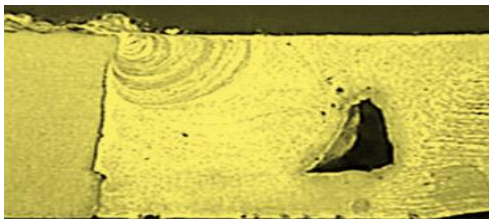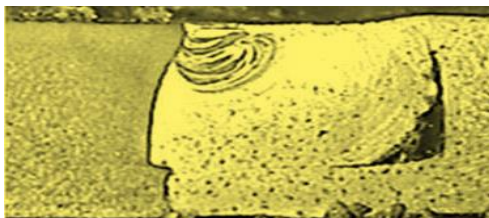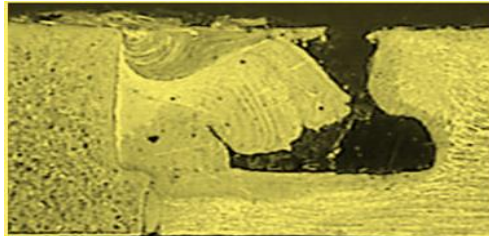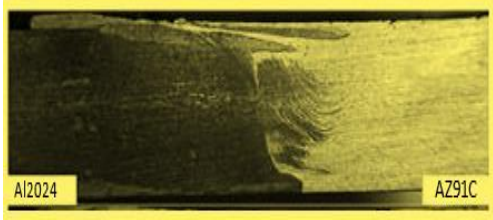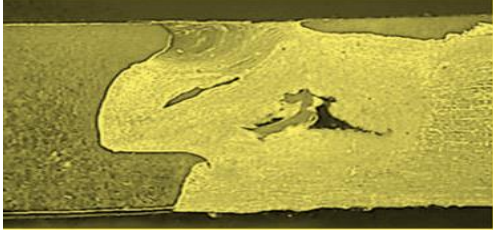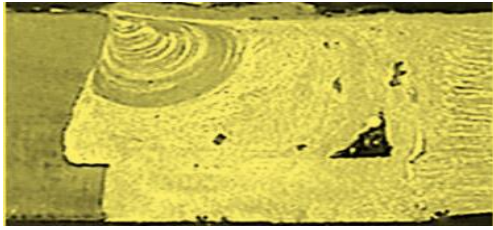
Sample	Joint appearance	Cross-sectional macrostructures
1	Crack	Al2024 AZ91C **1mm**
2	Kissing bond	
3	Grove	
4		
5	Tunneling	
6	Cavity	

Table 9. (*continued*)

| 7 | | |
| Sample 7 (W=1600 rpm, v=8 mm/min a=0.4 mm) | | No Defect |

Sample 7 (W=1600 rpm, v=8 mm/min a=0.4 mm)

No Defect

Tunneling

8

Tunneling

9

with rotational speed, velocity and plunge depth of 1600 rpm, 8 mm/min and 0.4 mm, respectively (Table 9).

3.3. Microstructure analysis

Sample 7 in Table 9 depicts the surface of the friction stir welded joint between aluminum 2024 and AZ91C metals, welded at a rotational speed of 1600 rpm and a Velocity of 8 mm/min. The joint surface exhibits slight unevenness and some flash around the joint area, attributable to deviation of the shoulder tool relative to the normal vector of the sheets.

Irrespective of the rotational speed, the tool shape influences heat input and weld quality, alongside the downward force applied by the tool. These factors collectively impact heat input and the attainment of defect-free joints. Initially, in this study, the downward force was set such that the back surface of the shoulder depressed approximately 0.2 mm into the sheets upon contact, persisting until the commencement of welding. The resulting microstructure, as illustrated in Fig. 7, reveals tunnel defects within the joint area, stemming from inadequate heat and improper stirring due to

insufficient penetration depth of the tool. Within these tunnel-shaped voids, insufficient process temperature impedes proper stirring, resulting in unmixed materials. Consequently, a 0.2 mm penetration depth is deemed unsuitable. To rectify these voids, a penetration depth of 0.4 mm was selected to eliminate such defects in subsequent joints.

Studies have shown that process parameters (rotation speed of tool, advance speed of tool, tool geometry) affect the microstructure and mechanical properties of the resulting friction stir weld. In order to obtain a proper weld quality, the heat input of the weld must have an optimum value. In this regard, the rotation and traverse speeds of the tool are among the parameters controlling the heat input of the weld. Insufficient heat input due to poor material flow causes defects such as lack of fusion and tunnel [22, 23].

Rotational and traversal speed are two main parameters of FSW process. The material is stirred and mixed by rotation and forward movement of tool. The thermal cycle's contribution has higher importance compared to material flow for the precipitation evolution
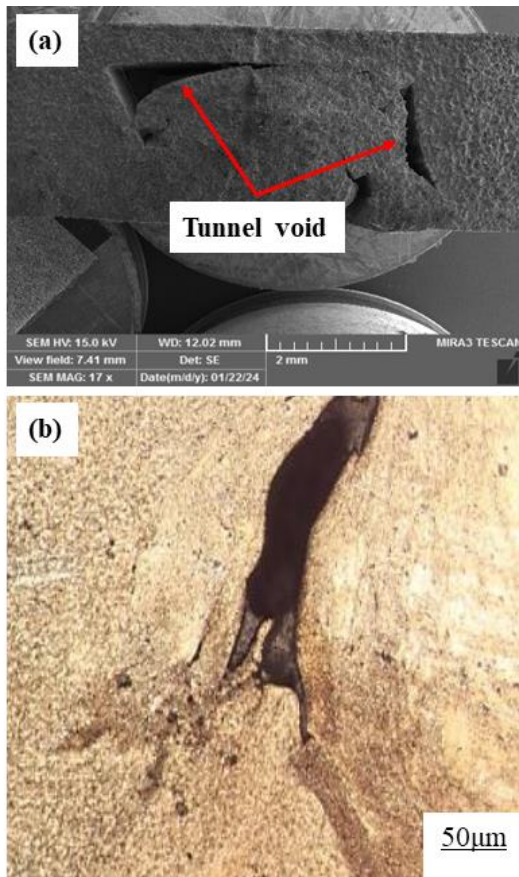
Fig. 7. Presence of tunnel defects in the weld joint due to improper penetration depth; (a) tunnel voids and (b) cavity at higher magnification.

of second phase particles.

Mishra et al. [3] proposed to estimate the heat input of FSW by using the following formula, Eq. (1):

$$Q = \frac{4}{3}\pi^2 \alpha \mu P R^3 \frac{\omega}{v} \tag{1}$$

Where Q is the heat input per unit of length and α, P, R and μ stand for heat input efficiency, pressure of tool on the joint, shoulder radius and friction coefficient, respectively while ω and v are the rotation and traverse speeds, respectively. It can be concluded that a relatively higher ω/v ratio can increase heat input so that more metal around the pin can reach plastic state, flow and deform with the pin rotation, and then recrystallize. Therefore, the areas of the stir zone and HAZ are relatively wider with higher ratio of ω/v [24].

Friction stir welding (FSW) is fundamentally based on thermodynamic changes, and the process temperature directly affects the microstructure of the welded area and the resulting mechanical properties. The magnitude of this temperature and its distribution in the workpiece are of particular importance. Depending on the process parameters such as rotational speed and traverse speed, this temperature will vary. However, in general, these parameters in FSW are set so that the temperature in the weld zone reaches about 80% to 90% of the metal's melting point. For friction stir welding, there is an empirical relationship that defines the correlation between the weld nugget temperature and process parameters [27, 30]:

$$\frac{T}{T_m} = K\left(\left(\frac{\omega^2}{V.10^4}\right)^a\right) \tag{2}$$

In this equation, T_m is the alloy melting temperature, T is the temperature in the weld nugget, ω is the tool rotational speed, v is the traverse speed, *a* and *K* are constant values that depend on the base metal material.

Higher heat input compared to the optimal joint, i.e., lower traverse speeds or higher rotational speeds, leads to the formation of thicker intermetallic compounds in the surface areas, which act as the origin of brittle fracture during tensile testing. At lower heat inputs, defects such as gaps are reasons for lower tensile strength and ductility of joints. However, the fracture of the optimal joint occurs from thin intermetallic compounds formed between magnesium particles and the aluminum matrix with a ductile mode by creating dimples. In fact, the formation of a defect-free joint, a surface area without high strength/intermetallic compounds with a serrated structure, and thin intermetallic compounds around aluminum pieces increase the strength and ductility of joints. The mechanism of microstructure formation in the stir zone (SZ) of the optimal joint includes dynamic recrystallization on the aluminum and magnesium sides, leading to the formation of fine and equiaxed grains, the formation of micro-cracks in aluminum, and their filling with magnesium.

The microstructure of the joint obtained from welding at 800 rpm rotational speed and 20 mm/min Velocity is shown in Fig. 8(a). As observed in the micro images, a layered structure has been formed in the stirred zone. This structure, which often occurs in dissimilar

alloy welds, is caused by insufficient mixing of the two materials due to low heat input. Layered or onion ring structures indicate differences in chemical composition and also differences in grain sizes [25]. In fact, in friction stir welding of dissimilar alloys, due to the fact that there is not enough time for element diffusion during welding, this structure is more commonly observed. In addition, if the heat input is low, the driving force required for element diffusion is lower and the layered structure occurs more intensely.
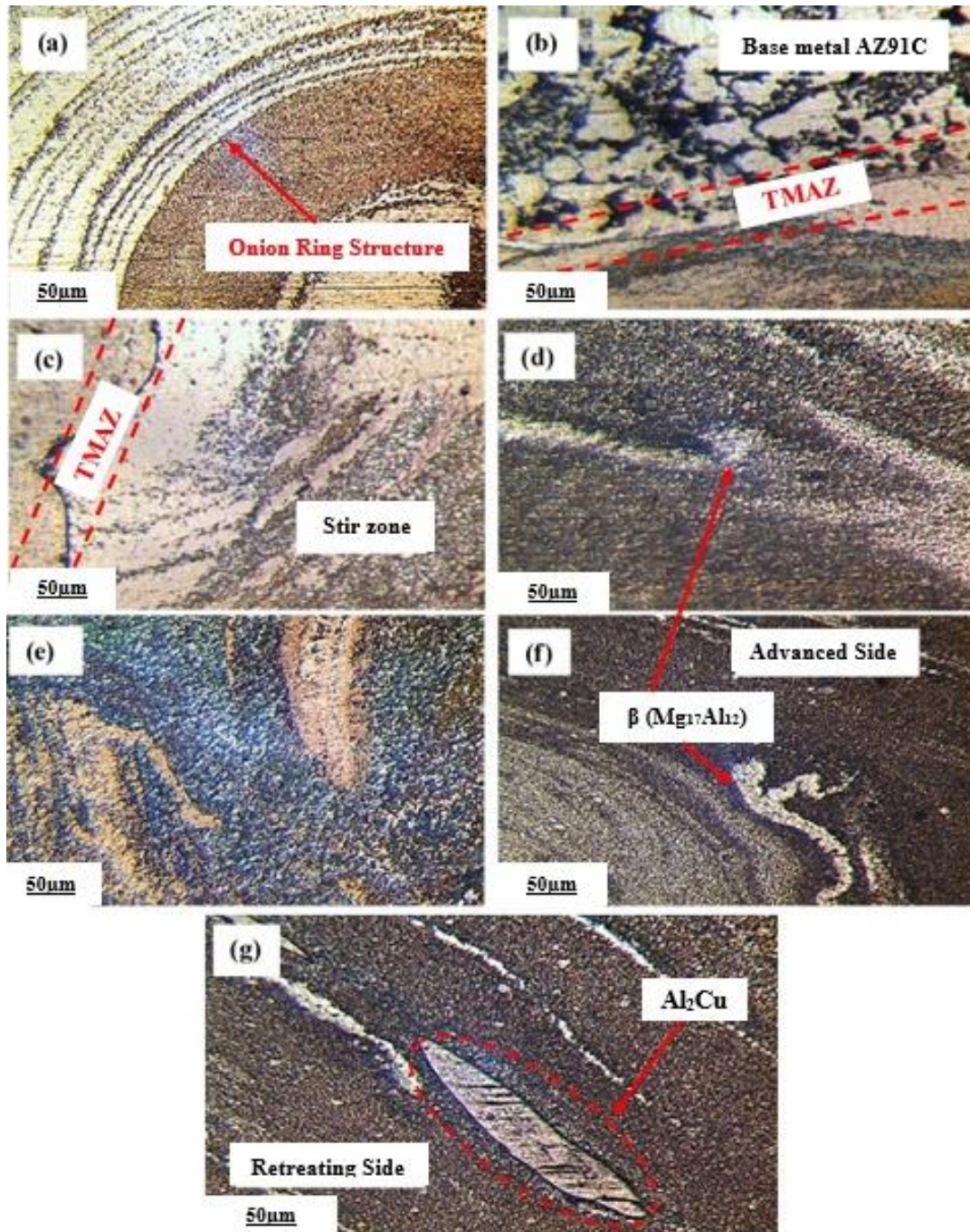

Fig. 8. The microstructure of the joint; (a) stir zone welding at 800 rpm rotational speed and 20 mm/min, (b) and (c) grain size and shape in the TMAZ region, (d) and (e) stir zone obtained with the parameters of 1600 rpm rotational speed and 8 mm/min, (f) and (g) stir zone area on both advancing and retreating sides.

The bright areas in Fig. 8(a) represent the Al2024 and the dark areas indicate the magnesium alloy AZ91C, which has been etched more intensely. In Fig. 8(b) and 8(c), the grain size and shape in the TMAZ region can be seen. As shown in these figures, the grains have been pulled down from the top of the stirred zone due to the tool pin rotation. Grain refinement does not occur in this region due to lack of sufficient strain and heat. The precipitates in the TMAZ region are relatively coarser than the stirred zone and more undissolved precipitates can be seen compared to the stirred zone. This type of grain structure in the TMAZ can be justified by considering the pin situation and tool rotation direction, in the sense that the material flows upwards in a square shape. In addition, during the process, the pin rotation causes the material to be transferred from the advancing side to the retreating side. Another point that is evident from the figures is the shape and size of the grains in the upper part of the TMAZ and the lower part of this region. As can be seen, due to the heat sink that exists in the lower part of the joint, the cooling rate is higher in this section, so recrystallization occurs to a lesser extent, hence more aligned and smaller grains are formed compared to the upper section [26]. In Fig. 8(d) and 8(e), the microstructure images of the stirred zone obtained with the parameters of 1600 rpm rotational speed and 8 mm/min linear speed on the advancing and retreating sides are shown, respectively. As can be seen in these figures, with increased heat input and concurrent severe plastic deformation, dynamic recrystallization has occurred in the stirred zone, which has led to grain refinement. Additionally, as evident, the grain size on the retreating side is smaller than on the advancing side. This is because during welding, the advancing side of the stirred zone experiences higher temperatures [27].

Moreover, with increased heat input, the existing alloying elements gain more driving force to diffuse, and the layered structure occurs less at high heat input, but due to the relatively high cooling rate this structure has not completely disappeared. In Fig. 8(f) and 8(g), the grain structures in the stirred zone area on both advancing and retreating sides are shown, respectively. As can be seen, the grains have been pulled down from top to bottom, grain refinement has occurred in this region and the grain size is much finer compared to the HAZ region. In the lower sections where the cooling rate is higher, recrystallization occurs to a lesser extent and aligned grains are also observed. According to the images, the pulled-down grains from top to bottom are evident in this region [28].

Fig. 8 clearly demonstrates how FSW process parameters (rotational and traverse speeds) influence the weld's microstructural evolution. Increasing the ratio of rotational speed to traverse speed leads to finer grain structures and more complex material flow patterns. These microstructural changes directly affect the joint's mechanical properties, corrosion resistance, and fatigue performance. Moreover, the notable differences between the advancing and retreating sides in terms of material flow and microstructural changes highlight the importance of optimizing process parameters to achieve a uniform and defect-free joint. This comprehensive microstructural analysis not only provides deep insights into the mechanisms governing the FSW process but also lays the groundwork for optimizing process parameters to achieve high-quality joints. This analysis provides a thorough understanding of the FSW process's microstructural aspects, serving as a foundation for further research and process optimization in the field of friction stir welding [21-29].

Microstructural analysis of the weld was also investigated using SEM. In order to accurately analyze the type of material flow in the weld zone, SEM images of the weld cross section surface were taken, the details of which are shown in Fig. 9. Fig. 9(a) shows the layered structure created in the central zone of the weld due to the flow of aluminum in the upper part of the weld zone which leads to the diffusion of magnesium towards aluminum from the advancing side due to the rotation of the tool pin. Fig. 9(b) shows a continuous and thin intermetallic layer at the junction of aluminum and magnesium. Furthermore, by carefully looking at Fig. 9(c), the dispersion of magnesium particles separated under the influence of heat and plastic deformations and their movement towards aluminum can be clearly seen, which indicates a composite structure of magnesium
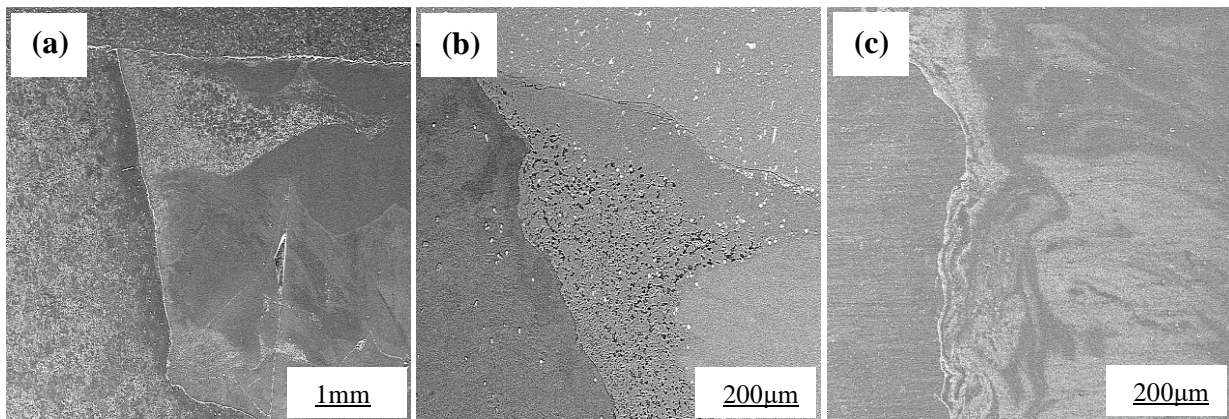
Fig. 9. (a) Cross section surface of welded sample, (b) continuous and thin intermetallic layer at the junction of aluminum and magnesium, and (c) dispersion of separated magnesium particles.

particles in an aluminum matrix in this region. The formation of intermetallic compounds in this region can be clearly seen. In addition, by carefully observing the image contrast and considering the proximity to aluminum and darker color, it can be inferred that it is the strengthening compound Al_2Cu.

3.4. Microhardness test

The microhardness data obtained from the weld centerline is depicted in Fig. 10. Generally, a material's hardness is characterized by its resistance to deformation. Microhardness, a form of sectional hardness measurement, is particularly sensitive to metal phases, work hardening, and measurement location, each of which can vary and thereby influence the measured hardness [29]. Given the segmented nature of the welded metals in this study, the microhardness at the junction between aluminum 2024 and magnesium AZ91C is divided into eight distinct parts, with corresponding bands delineated in Fig. 10.

Predominantly, the hardness of the joint is affected by process parameters. Variations in these parameters alter heat input and the size of the microstructure within the joint, consequently influencing joint hardness [29]. The hardness test results revealed that the highest hardness was attained in joints welded at a linear speed of 8 mm/min and a rotational speed of 1600 rpm, registering approximately 148 HV. This phenomenon is attributed to the fine-grained structure of the base metals

within the stirred zone.

Moreover, the arrangement of the two metals influences mechanical work rate and heat generation, particularly evident at low rotational speeds and high linear speeds. Under these conditions, dispersed magnesium particles become embedded in the aluminum base, enhancing joint hardness. Fig. 11(a) illustrates an instance of finely dispersed magnesium particles formed at 1250 rpm and 16 mm/min.

Conversely, simultaneous increases in rotational speed and reductions in linear speed result in a decrease in the microstructure size of the joint, facilitating the incorporation of larger magnesium particles into the stirred zone, as depicted in Fig. 11(b). Moreover, the heightened formation of intermetallic layers and layered composite structures at elevated rotational speeds and decreased linear speeds further contribute to increased hardness within the stirred zone and its surroundings.

Ultimately, the highest joint hardness was achieved through welding at a rotational speed of 1600 rpm and a Velocity of 8 mm/min, yielding a hardness measurement of approximately 148 HV.

The highest microhardness within the advancing side is notably concentrated at the center, attributable to the presence of $Mg_{17}Al_{12}$ and Al_2Cu precipitates within the weld zone [30]. This observation holds true across various samples, indicating a consistent trend. Notably, microhardness within the weld zone demonstrates a slight enhancement as the tool pin position shifts towards
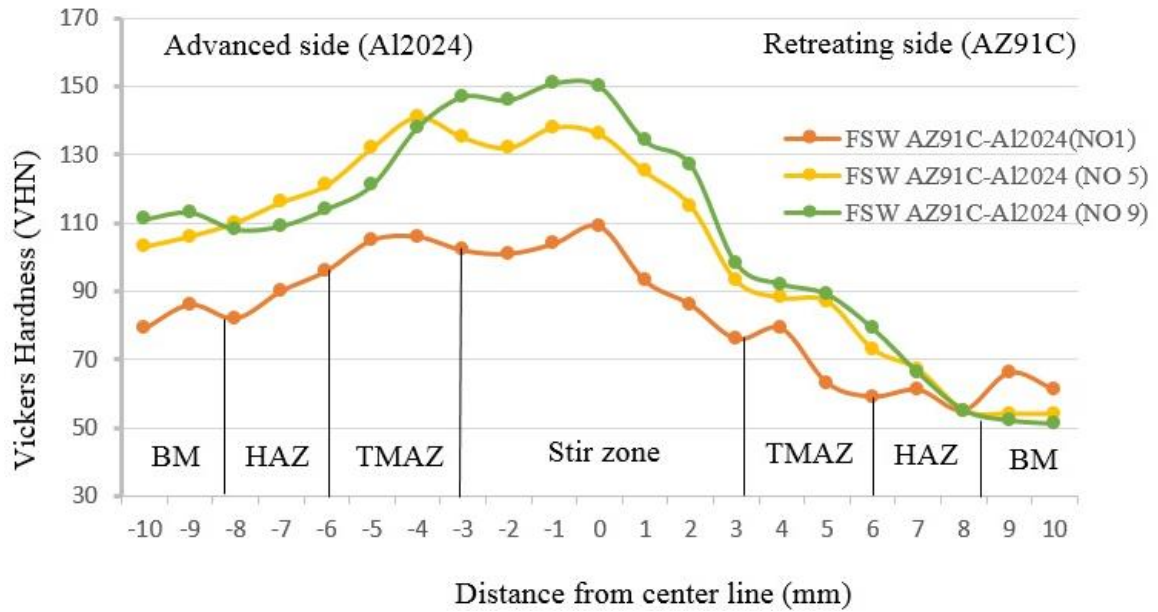
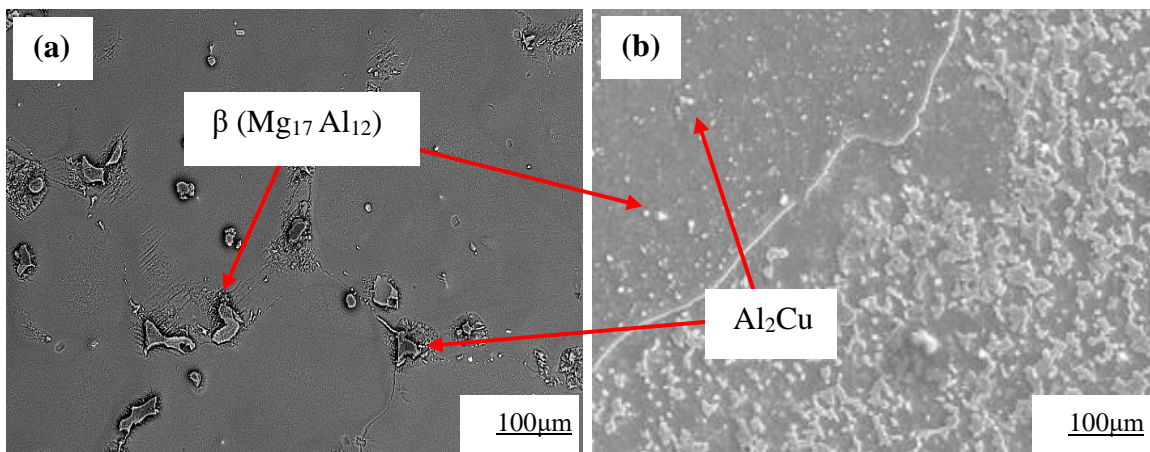**Fig. 10.** Microhardness of the sample welded by FSW method.

Fig. 11. (a) Sample welded at 1250 rpm and 16 mm/min traverse speed and (b) sample welded at 1600 rpm and 8 mm/min traverse speed.

the advancing side. Conversely, when the tool position leans towards the retreating side, microhardness in the weld zone diminishes, aligning with findings from the microstructural analysis. The formation of onion-shaped rings accompanied by a fine-grained structure notably contributes to heightened microhardness compared to the other samples.

4. Conclusion

In this study, we successfully performed dissimilar friction stir welding (FSW) on 5 mm thick aluminum alloy Al2024 and magnesium alloy AZ91C sheets. Using the Taguchi design of experiments, we optimized the

FSW process parameters tool rotational speed, welding speed, and plunge depth to maximize hardness within the weld zone. The optimal parameters were identified at a rotational speed of 1600 rpm, Velocity of 8 mm/min, and plunge depth of 0.4 mm, achieving a maximum hardness of 148 HV in the stir zone.

Microstructural analysis revealed a layered structure typical of dissimilar FSW joints due to limited elemental diffusion between the alloys. SEM analysis showed a continuous intermetallic layer at the interface and the dispersion of magnesium particles within the aluminum matrix, forming a composite-like structure in parts of the stir zone. Hardness distribution across the weld joint

corresponded to microstructural changes, with the highest hardness in the fine-grained stir zone, followed by the thermomechanically affected zone (TMAZ) and heat-affected zone (HAZ). Our findings highlight the effectiveness of FSW in joining Al2024 and AZ91C alloys, emphasizing the importance of optimizing process parameters to achieve desirable mechanical properties and microstructural features. The study provides insights into the microstructural characteristics and microhardness variations in FSW joints of aluminum and magnesium alloys. The increased microhardness within the weld zone with the tool pin position towards the advancing side (AS) was linked to the formation of fine-grained onion-shaped rings, whereas a decrease in microhardness was observed when the tool position shifted towards the retreating side (RS).

These results enhance the understanding of dissimilar FSW processes and underscore the necessity of precise parameter optimization for superior weld quality and mechanical performance. This research offers valuable guidance for aerospace and automotive industries, which use lightweight aluminum and magnesium alloys. Future research should further explore the relationships between microstructural features, mechanical properties, and welding parameters to advance the field of friction stir welding.

Conflict of Interest

There is no conflict of interest.

Funding

There is no funding available.

5. References

[1] Friedrich, H. E., & Mordike, B. L. (2006). *Magnesium technology: metallurgy, design data, applications.* Springer Berlin, Heidelberg. https://doi.org/10.1007/3-540-30812-1

[2] Lohwasser, D., & Chen, Z. (Eds.). (2009). *Friction stir welding: From basics to applications.* Elsevier.

[3] Mishra, R. S., & Mahoney, M. W. (2007*). Friction stir welding and processing.* ASM international.

[4] Liu, L. (2010). *Welding and joining of magnesium alloys.* Woodhead Publishing.

[5] Davis, J. R. (1990*). Properties and selection: nonferrous alloys and special-purpose materials.* ASM international.

[6] Czerwinski, F. (Ed.). (2011). *Magnesium alloys: design, processing and properties*. BoD–Books on Demand.

[7] Davis, J. R. (1993). *Aluminum and aluminum alloys.* ASM international.

[8] Venkateshkannan, M., Rajkumar, V., & Sadeesh, P. (2014). Influences of tool geometry on metallurgical and mechanical properties of friction stir welded dissimilar AA 2024 and AA 5052. *Procedia Engineering*, 75, 154-158. https://doi.org/10.1016/j.proeng.2013.11.033

[9] Prasad, B. L., Neelaiah, G., Krishna, M. G., Ramana, S. V. V., Prakash, K. S., & Pradeep Kumar Reddy, G. (2018). Joining of AZ91 Mg alloy and Al6063 alloy sheets by friction stir welding. *Journal of Magnesium and Alloys*, 6(1), 71-76. https://doi.org/10.1016/j.jma.2017.12.004

[10] Li, P., You, G., Wen, H., Guo, W., Tong, X., & Li, S. (2019). Friction stir welding between the high-pressure die casting of AZ91 magnesium alloy and A383 aluminum alloy. *Journal of Materials Processing Technology*, 264, 55-63. https://doi.org/10.1016/j.jmatprotec.2018.08.044

[11] Jabraeili, R., Jafarian, H. R., Khajeh, R., Park, N., Kim, Y., Heidarzadeh, A., & Eivani, A. R. (2021). Effect of FSW process parameters on microstructure and mechanical properties of the dissimilar AA2024 Al alloy and 304 stainless steel joints. *Materials Science and Engineering A*, *814*, 140981. https://doi.org/10.1016/j.msea.2021.140981

[12] Vuherer, T., Milčić, M., Glodež, S., Milčić, D., Radović, L., & Kramberger, J. (2021). Fatigue and fracture behaviour of friction stir welded AA-2024-T351 joints. *Theoretical and Applied Fracture Mechanics*, *114,* 103027. https://doi.org/10.1016/j.tafmec.2021.103027

[13] Hasani, B. M., Hedaiatmofidi, H., & Zarebidaki, A. (2021). Effect of friction stir process on the microstructure and corrosion behavior of AZ91 Mg alloy. *Materials Chemistry and Physics*, *267,* 124672. https://doi.org/10.1016/j.matchemphys.2021.124672

[14] Geyer, M., Vidal, V., Pottier, T., Boher, C., & Rezai-Aria, F. (2021). Investigations on the material flow and the role of the resulting hooks on the mechanical behaviour of dissimilar friction stir welded Al2024-T3 to Ti-6Al-4V overlap joints. *Journal of Materials Processing Technology*, *292,* 117057. https://doi.org/10.1016/j.jmatprotec.2021.117057

[15] Kumar, S. D., & Kumar, S. S. (2021). Effect of heat treatment conditions on ballistic behaviour of various zones of friction stir welded magnesium alloy

joints. *Transactions of Nonferrous Metals Society of China*, *31*(1), 156-166.
https://doi.org/10.1016/S1003-6326(20)65484-X

[16] Khajeh, R., Jafarian, H. R., Seyedein, S. H., Jabraeili, R., Eivani, A. R., Park, N., & Heidarzadeh, A. (2021). Microstructure, mechanical and electrical properties of dissimilar friction stir welded 2024 aluminum alloy and copper joints. *Journal of Materials Research and Technology*, *14*, 1945-1957.
https://doi.org/10.1016/j.jmrt.2021.07.058

[17] Kandasamy, J., Prakasham, G., Chaitanya, P., & Eshwar, N. (2023). Experimental investigations on the position of plates in friction stir welding of dissimilar alloys. *Materials Today: Proceedings*.
https://doi.org/10.1016/j.matpr.2023.08.296

[18] Rouhi, S., Mostafapour, A., & Ashjari, M. (2016). Effects of welding environment on microstructure and mechanical properties of friction stir welded AZ91C magnesium alloy joints. *Science and Technology of Welding and Joining*, *21*(1), 25-31.
https://doi.org/10.1179/1362171815Y.0000000058

[19] Rouhi, S., Dadashpour, M., Mostafapour, A., & Doniavi, A. (2017). Effects of multi-pass FSP on the β phase ($Mg_{17}Al_{12}$) distribution and mechanical properties of AZ91C magnesium alloy. *Journal of Achievements in Materials and Manufacturing Engineering*, *82*(2), 77-85.
https://doi.org/10.5604/01.3001.0010.2358

[20] Liu, C., Chen, D. L., Bhole, S., Cao, X., & Jahazi, M. (2009). Polishing-assisted galvanic corrosion in the dissimilar friction stir welded joint of AZ31 magnesium alloy to 2024 aluminum alloy. *Materials Characterization*, *60*(5), 370-376.
https://doi.org/10.1016/j.matchar.2008.10.009

[21] Rouhi, S., Doniavi, A., & Shahbaz, M. (2023). Exploring the impact of friction stir welding parameters on mechanical performance and microstructure of AZ91C magnesium alloy joints using taguchi method. *Iranian Journal of Materials Forming*, *10*(3), 4-14.
https://doi.org/10.22099/ijmf.2023.47437.1258

[22] Abdollahzadeh, A., Shokuhfar, A., Cabrera, J. M., Zhilyaev, A. P., & Omidvar, H. (2019). In-situ nanocomposite in friction stir welding of 6061-T6 aluminum alloy to AZ31 magnesium alloy. *Journal of Materials Processing Technology*, *263*, 296-307.
https://doi.org/10.1016/j.jmatprotec.2018.08.025

[23] Raturi, M., & Bhattacharya, A. (2023). Temperature variation and influence on local mechanical properties assessed by nanoindentation in AA6061-AA7075 dissimilar FSW. *International Communications in Heat and Mass Transfer*, *148*, 107079.
https://doi.org/10.1016/j.icheatmasstransfer.2023.107079

[24] Hu, Z., Yuan, S., & Wang, X. (2011). Effect of post-weld heat treatment on the microstructure and plastic deformation behavior of friction stir welded 2024. *Materials & Design*, *32*(10), 5045-5050.
https://doi.org/10.1016/j.matdes.2011.05.035

[25] Amancio-Filho, S. T., Sheikhi, S., Dos Santos, J. F., & Bolfarini, C. (2008). Preliminary study on the microstructure and mechanical properties of dissimilar friction stir welds in aircraft aluminium alloys 2024-T351 and 6056-T4. *Journal of Materials Processing Technology*, *206*(1-3), 132-142.
https://doi.org/10.1016/j.jmatprotec.2007.12.008

[26] de Viveiros, B. V. G., da Silva, R. M. P., Donatus, U., & Costa, I. (2023). Welding and galvanic coupling effects on the electrochemical activity of dissimilar AA2050 and AA7050 aluminum alloys welded by Friction Stir Welding (FSW). *Electrochimica Acta*, *449,* 142196.
https://doi.org/10.1016/j.electacta.2023.142196

[27] Rizehvandy, S., Salimi, M., & Nasiri, A. A. (2019). Finite element simulation of dynamic recrystallization phenomenon and evaluation of effective factors in friction stir welding in AA-2024 aluminum alloy. *Metallurgical Engineering*, *22*(4), 254-266.
https://doi.org/10.22076/me.2020.107411.1246

[28] Amancio-Filho, S. T., Sheikhi, S., Dos Santos, J. F., & Bolfarini, C. (2008). Preliminary study on the microstructure and mechanical properties of dissimilar friction stir welds in aircraft aluminium alloys 2024-T351 and 6056-T4. *Journal of Materials Processing Technology*, *206*(1-3), 132-142.
https://doi.org/10.1016/j.jmatprotec.2007.12.008

[29] Mir, F. A., Khan, N. Z., Parvez, S., & Siddiquee, A. N. (2024). Investigations on surface properties of friction stir welded dissimilar AA2024-T3 and 304 stainless steel joints. *Tribology International*, *193,* 109312.
https://doi.org/10.1016/j.triboint.2024.109312

[30] Pasetti-Roza, A., Victoria-Hernandez, J., da Cunha, P. H. C. P., de Lima Lessa, C. R., Bergmann, L. A., Kurz, G., & Klusemann, B. (2024). Behavior of microstructure and mechanical properties in the stir zone of friction stir welded ME21 magnesium alloy. *Journal of Materials Research and Technology*, *29*, 4895-4901.
https://doi.org/10.1016/j.jmrt.2024.02.188